RESEARCH ARTICLE

*Tc*BDF6 deficiency compromises intracellular amastigote development and infectivity in *Trypanosoma cruzi*

Victoria Boselli[1], Virginia G. Perdomo[2,3], Florencia Pacini[4], Juan A. Cueto[5], Alejandro Pezza[1], Patricia S. Romano[5,6], Roberto Docampo[7], Ana Rosa Perez[4,8], Esteban C. Serra[1,2] *.

1.Instituto de Biología Molecular y Celular de Rosario, IBR-CONICET, Rosario, Santa Fe, Argentina. **2.**Facultad de Ciencias Bioquímicas y Farmacéuticas, Universidad Nacional de Rosario, Rosario, Santa Fe, Argentina. **3.**CONICET, Rosario, Argentina. **4.**Instituto de Inmunología Clínica y Experimental de Rosario, IDICER-CONICET, Rosario, Santa Fe, Argentina. **5.**Laboratorio de Biología de *Trypanosoma cruzi* y la célula hospedadora, Instituto de Histología y Embriología (IHEM) "Dr. Mario H. Burgos", Mendoza, Mendoza, Argentina. **6.**Facultad de Ciencias Médicas, Universidad Nacional de Cuyo, Mendoza, Mendoza, Argentina. **7.**Center for Tropical and Emerging Global Diseases and Department of Cellular Biology, University of Georgia, Athens, GA, USA. **8.**Centro de Investigación y Producción de Reactivos Biológicos (CIPReB), Facultad de Ciencias Médicas, Universidad Nacional de Rosario, Rosario, Santa Fe, Argentina.

* serra@ibr-conicet.gov.ar

Citation:

Editor:

Copyright:

Data Availability Statement: The raw and processed data supporting this research are available at: https://doi.org/10.57715/UNR/QKLDVR , RDA UNR

Funding: This research was supported by FONCyT, (PICT-2020 SERIEA-017049), Universidad Nacional de Rosario (80020190300048UR); ASaCTeI, (PEICID-2023-115); Research Council United Kingdom (MR/P027989/1) and GlaxoSmithKline.

Competing interests: The authors have declared that no competing interests exist.
and reproduction in any medium, provided the original author and source

Abstract

Trypanosoma cruzi, the causative agent of Chagas disease, relies on complex gene regulatory mechanisms to adapt to its diverse host environments. Although this parasite lacks canonical transcriptional control, epigenetic regulation plays a pivotal role in modulating gene expression. Bromodomain-containing factors (BDFs), known for recognizing acetylated lysines on histones, have emerged as key regulators of chromatin structure and gene activity. Among the eight predicted BDFs in *T. cruzi*, *Tc*BDF6 is part of a TINTIN-like complex with *Tc*MRGx and *Tc*MRGBP, homologous to components of the NuA4/TIP60 chromatin remodeling complex. To investigate the function of *Tc*BDF6, we generated knockout (KO) parasites using CRISPR/Cas9 gene editing. While BDF6-deficient epimastigotes did not exhibit very significative growth differences, the resulting metacyclic trypomastigotes displayed drastically reduced infectivity. Strikingly, once inside host cells, *Tc*BDF6 deficient parasites differentiated into amastigotes but failed to replicate. This intracellular arrest was partially reversed by episomal re-expression of *Tc*BDF6. Consistently, BDF6 KO parasites also exhibited impaired infectivity, a defect that was also rescued in the add-back line. Our findings highlight *Tc*BDF6 as a critical regulator of intracellular parasite development, operating in stages beyond epimastigotes where epigenetic plasticity is essential for host adaptation. The unique, stage-specific phenotype of BDF6 knockouts underscores its functional importance and suggests that bromodomains may represent novel therapeutic targets against *T. cruzi*.

Author Summary

To survive in the dramatically different environments of its life cycle, *Trypanosoma cruzi,* the parasite that causes Chagas disease, must finely tune its gene expression. Unlike many organisms, *T. cruzi* lacks classical transcriptional regulation and instead relies on epigenetic mechanisms. Among the proteins involved in this regulation are bromodomain containing factors, which interpret chemical marks on chromatin. In this study, we focused on *Tc*BDF6, a bromodomain protein thought to be part of a chromatin remodeling complex. Using CRISPR/Cas9, we disrupted the *TcBDF6* gene and discovered that, while the mutant parasites could still form infective stages, they failed to replicate inside host cells. Reintroducing *TcBDF6*, it was rescued this defect, confirming its critical role in intracellular development. Our findings highlight the importance of epigenetic control in parasite survival and suggest that bromodomain proteins could be valuable targets for future treatments against Chagas disease.

Introduction

Trypanosoma cruzi is the etiological agent of Chagas disease, which affects approximately 7 million people globally. Among those infected, 20–30% develop severe clinical manifestations [1]. While historically confined to Latin America, migration has facilitated its spread to non-endemic regions, where transmission occurs via blood transfusion, organ transplantation, and congenital routes [2]. Protozoan parasitic infections, including those caused by *T. cruzi*, remain a significant public health challenge, particularly in developing countries. The drug resistance, along with the limited and often side-effect-prone therapeutic options, highlights the urgent need for novel therapeutic targets [3].

The life cycle of *T. cruzi* involves both vertebrate and invertebrate hosts, transitioning through extracellular and intracellular stages [4]. The infection begins with metacyclic trypomastigotes, released into the feces of a triatomine vector during a blood meal from a vertebrate. They reach the bloodstream through skin cuts or the mucosa and invade different cell types in the mammalian host. Once in the cytoplasm, they differentiate into replicative amastigotes, which undergo several rounds of division before differentiating again into trypomastigotes and bursting out of the host cell. Bloodstream trypomastigotes, ingested by the vector during a blood meal, differentiate into epimastigotes and replicate in the insect midgut. Such a complex life cycle, involving several morphologically and biochemically distinct parasite forms and different host environments, requires complex regulatory mechanisms to direct gene expression and the adaptive strategies that enable parasites to thrive within distinct hosts. [5]

Unlike most eukaryotic cells, *T. cruzi* exhibits polycistronic transcription of protein-coding genes within transcriptional units (PTUs) and lacks canonical promoters or regulatory transcription factors [6]. Due to this phenomenon, fine regulation of gene expression occurs through post-transcriptional mechanisms [7]. Despite this, chromatin remodeling through covalent histone modifications and/or histone variants regulates transcription initiation [8]. Many, but not all, of the epigenetic mechanisms that regulate chromatin structure to control DNA accessibility—and consequently transcription, replication, and repair—are conserved across eukaryotes [9]. In kinetoplastids, the study of epigenetics is still in its early stages, but these mechanisms are already considered crucial for parasite adaptation and virulence. [10]

Bromodomains (BDs) are ~110 amino acid protein modules that specifically bind to acetylated lysines (AcK) and are considered typical "readers" of histone epigenetic marks.

They consist of a four-α-helix bundle (αA, αB, αC, αZ) connected by loops that form a hydrophobic pocket essential for AcK recognition [9,11]. Upon recognizing AcK, BDs can act as scaffolds, acting together with other factors into complexes that regulate key nuclear activities like transcription, DNA repair, and replication. In mammals, alteration in BD function can lead to cell death or uncontrolled proliferation, and BD factors are often upregulated in cancers and chronic inflammatory diseases, making them potential drug targets [12].

T. cruzi genome encodes eight bromodomain-containing proteins (*Tc*BDF1–8), each with distinct features. When BDF1-3 knockout was attempted using CRISPR/Cas9 gene editing, it was only possible to obtain heterozygous mutants, which indicates that these proteins are essential at least for the epimastigote stage [13]. The expression of dominant-negative mutants provided additional evidence of the essentiality of these bromodomain-containing proteins [13–15]

Among the eight *T. cruzi* BDs, *Tc*BDF6 is highly divergent, with a unique 57-residue insertion in its AB loop and reduced similarity to canonical BDs. Despite the BD, *Tc*BDF6 does not possess any additional recognizable domain. We have previously shown that it can interact with two other proteins, we call *Tc*MRGx (containing a MORF4-related gene domain) and *Tc*MRGBP, to form a complex like the TINTIN complex from yeast and mammals [16]. By AF-2 modeling and yeast two-hybrid assays, we demonstrated that the BC loop of BD6 is involved in the interaction with *Tc*MRGBP, which itself interacts with TcMRGx in a similar way that in yeast and mammals these components do [17]. The evident structural conservation of *Tc*TINTIN contrast with the low sequence similarity of BDF6, *Tc*MRGx and *Tc*MRGBP with their equivalents from *Saccharomyces cerevisiae* (EAF5, EAF3, EAF7) or humans (BRD8, MRG15, MRGBP). TINTIN is an integral module of the essential yeast lysine acetyltransferase complex NuA4 that plays key roles in transcription regulation and DNA repair. Even though its function is not entirely understood, TINTIN works as an independent sub-complex that can interact and modulate NuA4 activity, the only acetylase complex that is essential in yeast. [18].

Trypanosomatids cause several diseases, evolving diverse mechanisms to differentiate along their life cycle and evade the host immune system, some of which are controlled by epigenetic mechanisms [19]**.** Despite the increasing interest in epigenetic mechanisms in protozoan [20], the functional roles of bromodomain-containing proteins in *T. cruzi* remain poorly characterized. While previous studies have addressed essentiality in the epimastigote stage for some BDFs **,** their contributions to vertebrate stages, particularly the intracellular amastigotes, remain unknown. Understanding the epigenetic regulation of these stages is critical, as amastigotes are responsible for chronic infection and pathology.

Comparative transcriptomic analyses between virulent and attenuated *T. cruzi* strains have revealed differential expression of genes involved in energy metabolism, oxidative stress response, and cell cycle regulation—key processes for parasite fitness and survival [22]. These findings underscore the importance of gene expression plasticity in shaping parasite phenotypes and raise the possibility that chromatin-associated proteins, such as BDFs, may contribute to this regulation by modulating gene expression profiles in response to environmental cues.

In this work we obtained KO parasites for the gene *TcBDF6,* that grow almost normally as epimastigotes. However, *Tc*BDF6 deficiency compromises both host-cell infection and amastigote development in cell cultures. Even though *TcBDF6* $^{-/-}$ parasites have high metacyclogenesis efficiency, the trypomastigotes obtained have low infectivity and, once

inside the cells, they transform into amastigotes within the parasitophorous vacuole and stop multiplying. This phenomenon is reversed by the episomal expression of the *TcBDF6* gene (add-back strain). Finally, KO parasites show deficiencies to infect mice, an effect that is also mitigated in the add-back strain.

These findings provide insights into the relevance of epigenetic mechanisms in parasite development and may lead to designing new therapeutic strategies targeting BD-containing proteins. Although functional studies on BDFs in *T. cruzi* are still limited, the unique phenotype of *TcBDF6* $^{-/-}$ points to its potential importance in the parasite's biology and pathogenesis.

Results

*Tc*BDF6 is not essential in the epimastigote stage

By using CRISPR/Cas9-mediated genome editing and cloning, we obtained a heterozygous (*TcBDF6* $^{-/+}$) and two homozygous (*TcBDF6* $^{-/-}$) knockout clones. Knockout strategy and PCR analysis of the clones are shown in S1 Fig. Since both complete knockouts showed identical phenotypes after evaluation (see below), clone A was used to generate a complemented strain by reintroducing a version of the *TcBDF6* gene modified to avoid recognition by the CRISPR-Cas9 system (named thereafter *TcBDF6* $^{-/-}$pBDF6 or just addback strain).

KO strain showed slower duplication time in epimastigotes stage

To assess whether the absence of *Tc*BDF6 affects *T. cruzi* epimastigote proliferation, we performed *in vitro* growth curve assays for five parasite lines: WT Dm28c, heterozygous mutant (*TcBDF6* $^{-/+}$), two independent BDF6 knockout clones (*TcBDF6* $^{-/-}$ Clone A and Clone B), and the addback line (*TcBDF6* $^{-/-}$ pBDF6).

As can be observed in Fig 1.A, the *TcBDF6* knockout clones displayed a consistently slower growth rate compared to WT and heterozygous parasites, with delayed entry into the exponential phase and reduced parasite densities at later time points. To quantify these differences, linear regression analyses were performed using data points from the exponential growth phase (48–120 hours), and duplication times were calculated. Both *TcBDF6* $^{-/-}$ clones exhibited significantly longer duplication times than the WT Dm28c strain, and the heterozygous mutant showed an intermediate phenotype (Fig. 1.B). The addback line partially restored the growth defect, achieving replication kinetics assimilable to hemizygous strain. This result is not surprising since the *pTEX* expression cannot be easily regulated [23]. In several attempts, we used different concentrations of hygromycin in the culture, but we never obtained the growing rate of the WT strain (not shown). All these findings demonstrate that *Tc*BDF6 is not essential for growth but contributes to optimal epimastigotes proliferation under culture conditions.

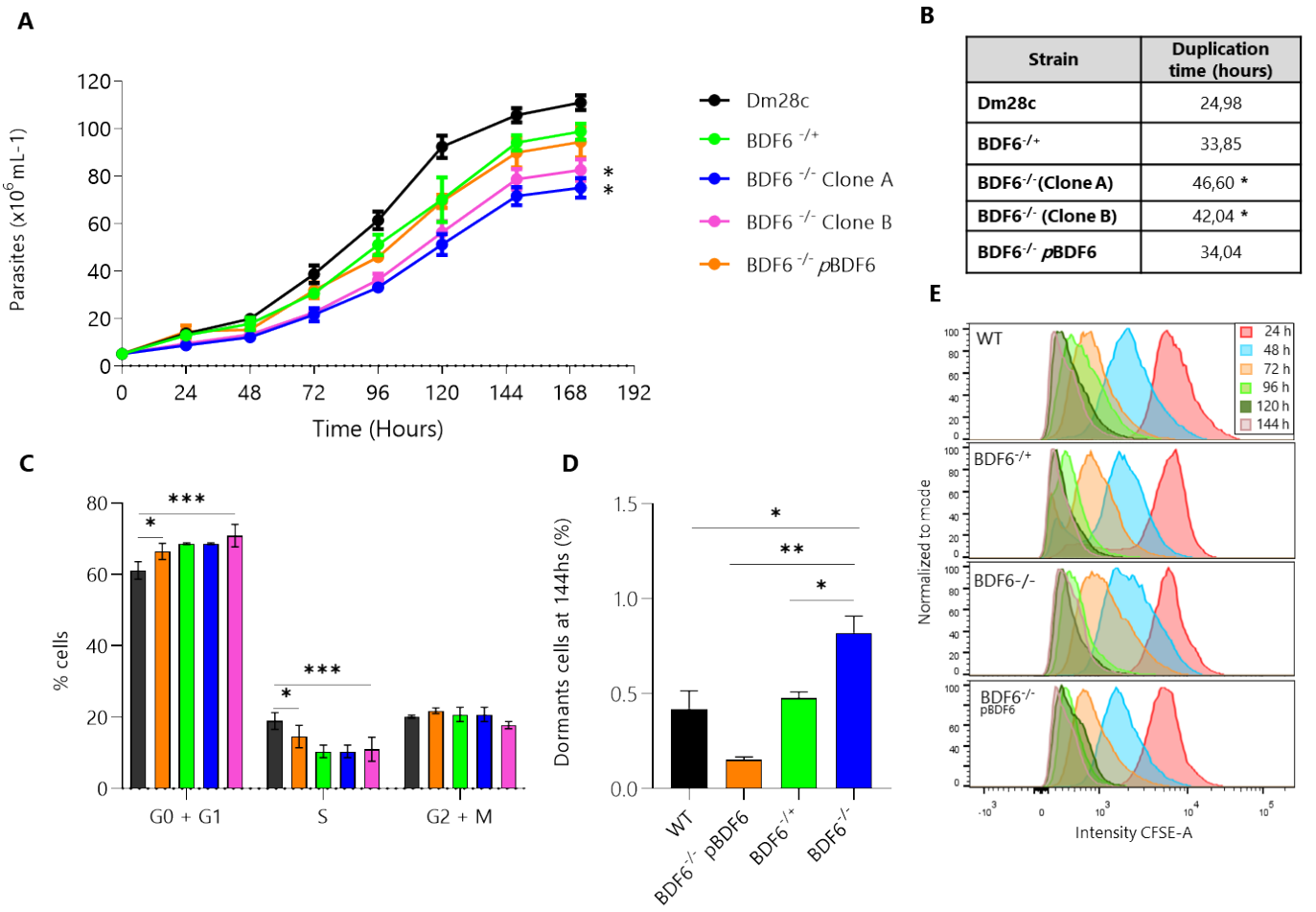

Strain	Duplication time (hours)
Dm28c	24,98
BDF6$^{-/+}$	33,85
BDF6$^{-/-}$(Clone A)	46,60 *
BDF6$^{-/-}$ (Clone B)	42,04 *
BDF6$^{-/-}$ *p*BDF6	34,04

Fig 1. Deletion of *TcBDF6* impairs epimastigote replication but affect cell cycle progression. A. Growth curves and **B.** Duplication times show that *TcBDF6* $^{-/-}$ epimastigotes exhibit a markedly reduced replication rate compared to wild-type (Dm28c), heterozygous (BDF6$^{-/+}$), and addback (BDF6$^{-/-}$ pBDF6) lines. Both *TcBDF6*$^{-/-}$ clones A and B displayed significantly prolonged duplication times (46.6 h and 42.0 h, respectively) relative to controls, indicating a replication defect due to BDF6 loss. This phenotype was largely rescued upon re-expression of *TcBDF6*. **C. Cell cycle at 72 h** indicate differences in cell among the strains, suggesting that the reduced growth is not attributable to increased cell death or early apoptosis-like processes. Together, these results implicate BDF6 in supporting optimal proliferation of *T. cruzi* epimastigotes **D. Dormancy in epimastigotes.** The average percentage of dormant cells in the experimental group strains at 144 h was detected in flow cytometry histograms. **E. Flow cytometry histograms.** Epimastigotes cultures of each strain from 24 to 144 h. CFSE intensity was assessed every 24 h until 144 h, and arrested cells were considered those ones which exhibited similar CFSE intensity at 144 h when compared to the level of half median of 24 h. Statistical analysis was performed using one-way ANOVA followed by Tukey's test (*p<0.05, **p<0.01, ***p<0.001, ****p<0.001 compared to WT).

To investigate the potential cause of the reduced proliferation observed in *TcBDF6* $^{-/-}$ parasites, we performed cell cycle analysis at 72 hours' post-inoculation. As shown in Fig 1.C, a significantly higher proportion of *TcBDF6* $^{-/-}$ parasites (Clone A and Clone B) are accumulated in the G_0/G_1 phase compared to WT and heterozygous strains, suggesting a cell cycle arrest or delay at this checkpoint. Correspondingly, the percentage of cells in S phase was markedly lower in both KO clones, while the G_2/M populations remained comparable across all lines. Notably, re-expression of TcBDF6 in the addback line restored the G_0/G_1 and S phase distribution to levels like those observed in the heterozygous strain. The data support a model in which loss *of TcBDF6* causes a cell cycle delay at the G_1/S transition, restricting entry into S phase and thus compromising epimastigotes proliferation.

Given the reduced growth rate observed in *TcBDF6* $^{-/-}$ parasites, we investigated whether this phenotype could result from a higher proportion of non-dividing, dormant cells. To assess this, we performed a CFSE-based dormancy assay as described by [24], evaluating epimastigotes from four experimental groups over a 144-hour period. The *TcBDF6* knockout clone A exhibited a significantly increased percentage of CFSE stained cells at 144 h compared to WT (Dm28c) and addback parasites. The heterozygous *TcBDF6* $^{-/+}$ strain displayed an intermediate profile, consistent with a possible gene dosage effect (Fig 1.D and 1.E). Notably, the addback line showed fewer dormant parasites than the WT. These results suggest that *TcBDF6* contributes to sustaining parasite proliferation and limiting dormancy entry in epimastigotes, which is consistent with the accumulation of parasites at G_0/G_1 previously observed. However, since the proportion of dormant cells remains below 1% even in *TcBDF6*$^{-/-}$ parasites, this subtle increase is unlikely to be the main driver of the observed growth impairment.

TcBDF6 knockout epimastigotes are smaller than those from the wild-type strain

As shown in Fig 2.A, all lines of parasites observed with ultra-expansion microscopy exhibit a conserved morphology, with no apparent granulation or structural abnormalities. The overall distribution of chromatin was also preserved. However, KO parasites appeared smaller than wild-type parasites. To examine this difference in greater detail, we conducted an automated analysis of parasite size using images of Giemsa-stained parasites. Fig 2.B shows the parasite sizes, expressed as surface area in the images. *TcBDF6* $^{-/-}$, *TcBDF6* $^{-/+}$, and addback parasites displayed significantly smaller sizes compared to WT parasites. *TcBDF6* $^{-/+}$ and add-back parasites exhibited an intermediate phenotype, falling between *TcBDF6* $^{-/-}$ and wild-type in terms of size. These size differences were also reflected in the light scattering values obtained from cytometry experiments designed to determine the cell cycle stages of the steady-state cultures (not shown).

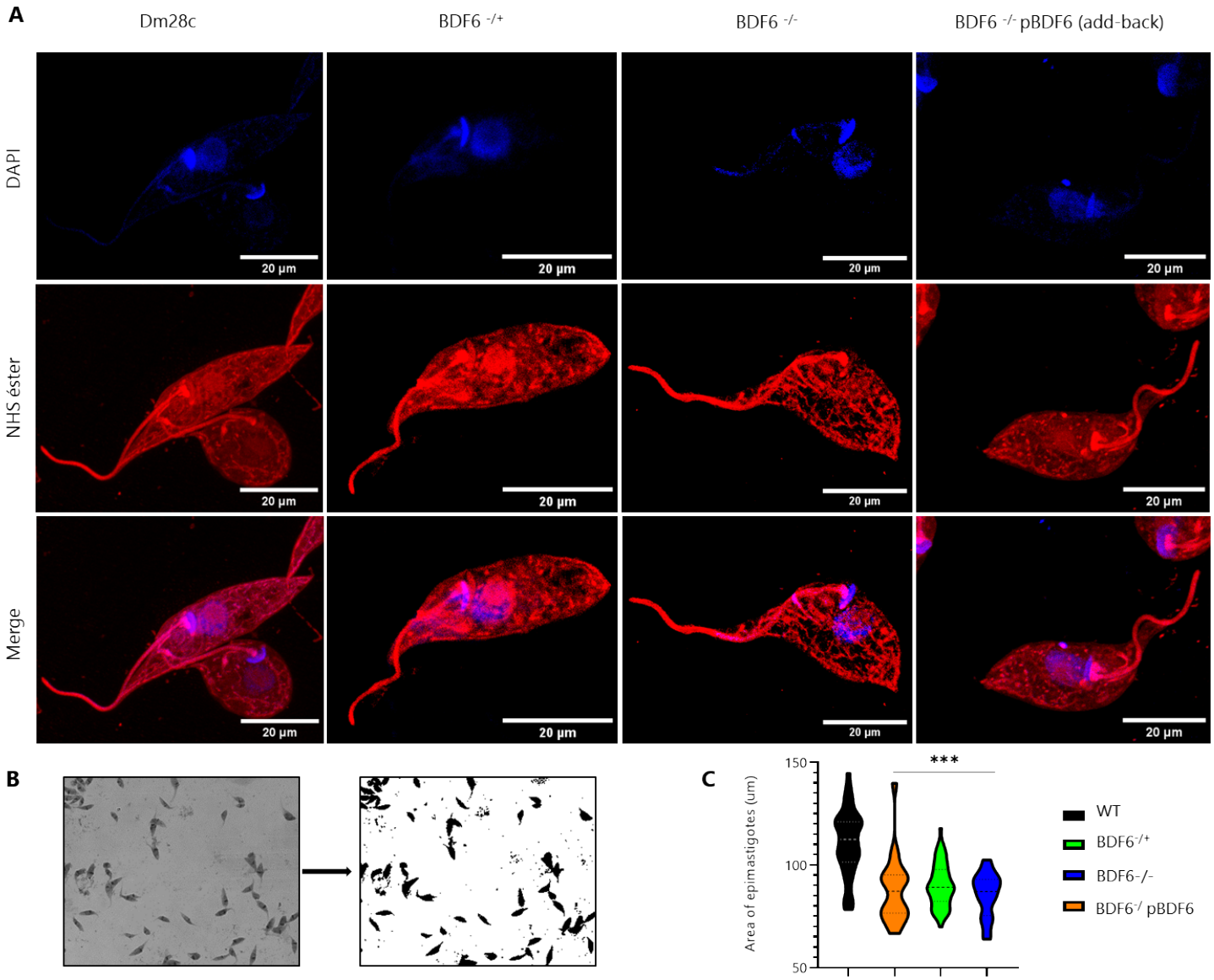

Fig 2. A. Ultra-Expansion Microscopy (U-ExM) of epimastigotes. Representative images of epimastigotes from *T. cruzi* Dm28c WT, heterozygous (*TcBDF6* $^{-/+}$), knockout (*TcBDF6* $^{-/-}$), and addback (*TcBDF6* $^{-/-}$ pBDF6) strains processed by Ultra-Expansion Microscopy (U-ExM). Parasites were stained with DAPI to visualize nuclear and kinetoplast DNA (blue), and with NHS ester to label proteins (red). Images are maximum intensity projections of expanded parasites, scale bar = 20 µm. **B. Giemsa-stained epimastigotes image processing.** Brightfield images (left) were processed using ImageJ to generate binary masks (right) by applying an automatic threshold, allowing for accurate segmentation and measurement of individual parasite areas. **C. Quantification of epimastigotes cell surface area.** Violin plot representing the area (in µm^2) of epimastigotes forms from WT, heterozygous (*TcBDF6* $^{-/+}$), knockout (*TcBDF6* $^{-/-}$), and addback (*TcBDF6* $^{-/-}$ pBDF6) strains. Cell surface areas were quantified from microscope images using ImageJ. A statistically significant difference was observed between the WT and all other experimental strains ($P < 0.0001$), while no significant differences were detected among the mutants and addback strains. Violins indicate median and interquartile ranges.

BDF6 deficient metacyclic trypomastigotes exhibit comparable morphology but differ in infectivity rates

The metacyclogenesis assay, we observed that the three mutant strains *TcBDF6* $^{-/-}$, *TcBDF6* $^{-/-}$ (Clone A), *TcBDF6* $^{-/-}$ (Clone B) showed similar percentages of metacyclogenesis than WT Dm28c (S2 Fig).

MT parasites have no morphological alterations when observed un ultra-expansion microscopy (Fig 3). Despite their conserved morphology, trypomastigotes from mutant strains revealed to be functionally altered. As shown in Fig 4.A and 4.B, the infection rate of the WT strain ranged between 15% and 20% of the cells. In contrast, the infection rate for the hemizygous and addback strains was reduced to around 5%, and dropped to less than 1% for the homozygous mutant strain. These findings suggest that, despite their external similarity, the absence of *Tc*BDF6 significantly impairs the infection capability of metacyclic trypomastigotes.

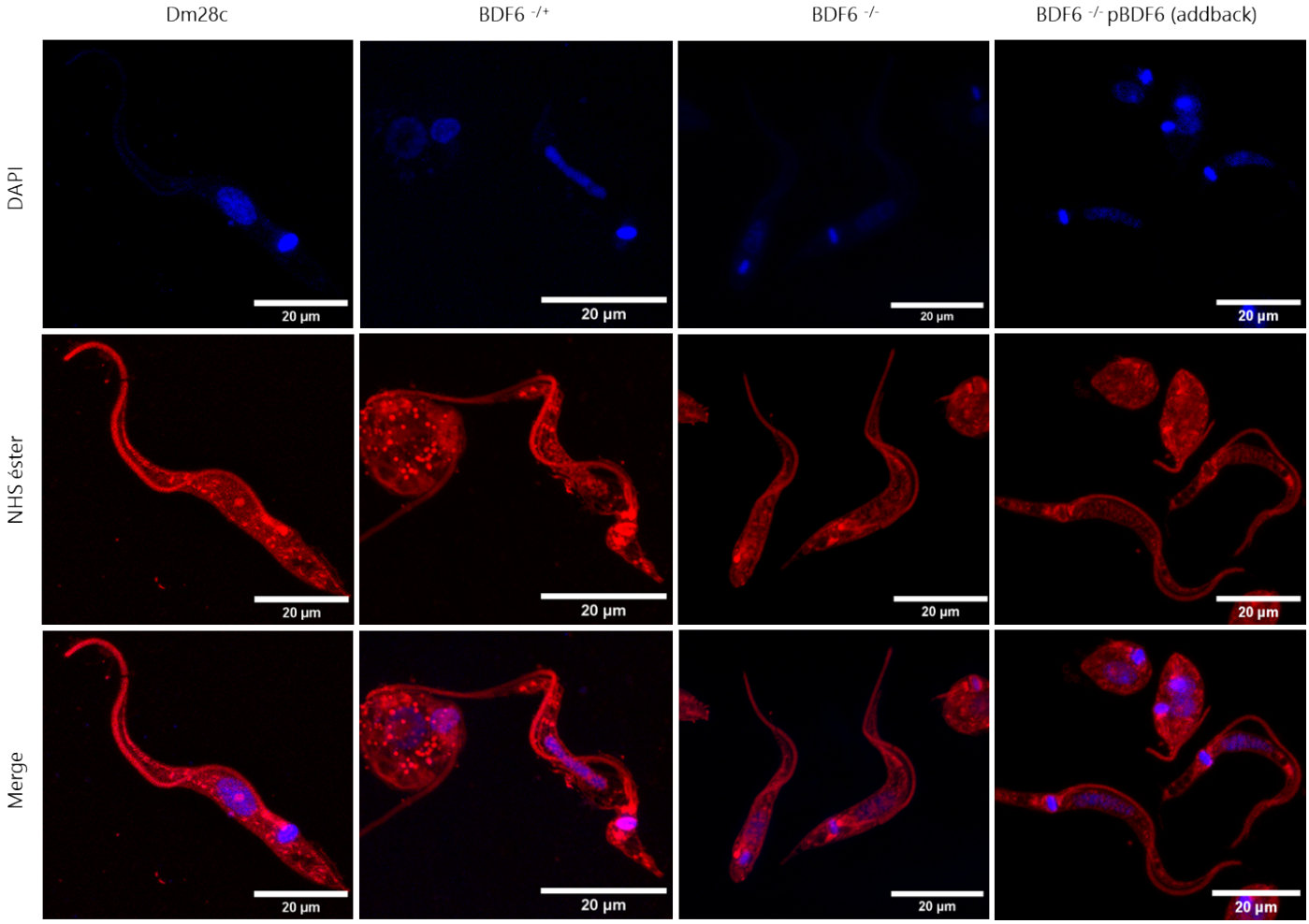

Fig 3. Ultra-Expansion Microscopy (U-ExM) of metacyclic trypomastigotes. Representative UExM images of Dm28c WT, heterozygous (*TcBDF6* $^{-/+}$), knockout (*TcBDF6* $^{-/-}$), and addback (*TcBDF6* $^{-/-}$ pBDF6) strains, stained with Alexa Fluor™ NHS ester (red), which labels surface and accessible proteins, and DAPI (blue), which stains DNA. Scale bars: 20 µm

Amastigote replication is compromised in the absence of *Tc*BDF6

We quantified the number of amastigotes that the different parasite lines develop per infected Vero cell. As shown in panel Fig 4.C, the WT Dm28c strain displayed a higher number of amastigotes per cell an average of 15 amastigotes, indicative of efficient intracellular replication. In contrast, the *TcBDF6* $^{-/-}$ mutants exhibited a strong reduced number of amastigotes, which was just one per cell. Interestingly, the addback strain showed partial recovery of the intracellular amastigote load, similar to the observed to the *TcBDF6* $^{+/-}$strain. Furthermore, it was observed that the number of amastigotes of the *TcBDF6* $^{-/-}$ strain did not increase and no trypomastigotes were released after 11 days of infection (data not

shown). These results highlight the importance of BDF6 not only for initiating infection but also for sustaining amastigote proliferation within host cells.

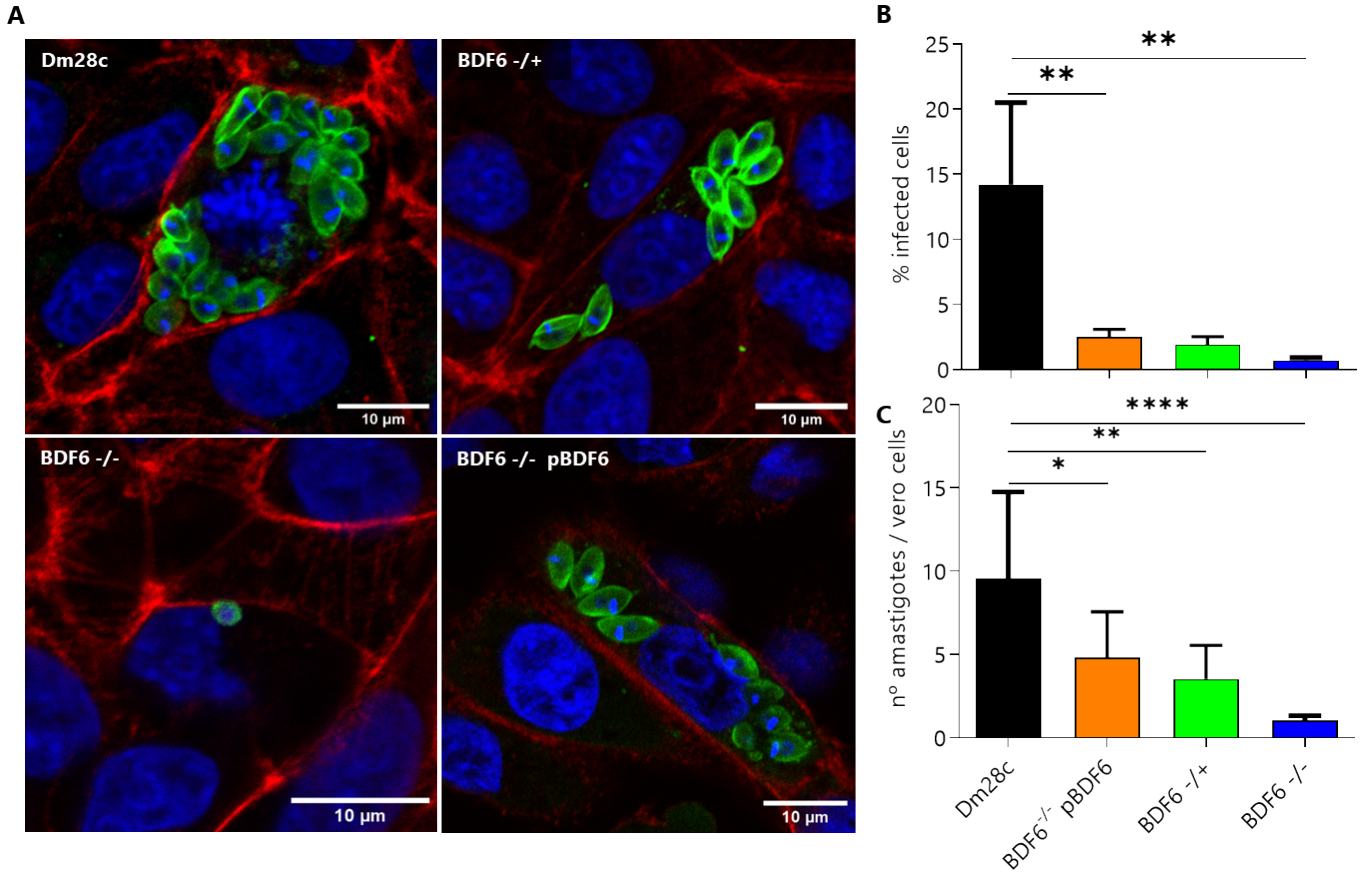

Fig 4. A. *In vitro* Vero cell infections. Representative confocal images of Vero cells infected with *T. cruzi* Dm28c WT, heterozygous (*TcBDF6* $^{-/+}$), knockout (*TcBDF6* $^{-/-}$), and addback (*TcBDF6* $^{-/-}$ pBDF6) strains. Intracellular amastigotes were visualized 72 hours pi. Parasites were stained with anti-*T. cruzi antibody* (green), host cell actin was labeled with phalloidin (red), and nuclei were counterstained with DAPI (blue). WT parasites shows infections with numerous amastigotes, whereas *TcBDF6* $^{-/-}$ mutants showed a dramatic reduction in intracellular replication, showing only one amastigote per cell. The addback strain partially rescued the phenotype. Scale bars = 10 µm **(B) Quantification of infection rates (% of infected Vero cells)** across the different strains. *TcBDF6* $^{-/+}$ and *TcBDF6* $^{-/-}$ mutants exhibited significantly reduced infection rates compared to WT. Complementation restored infectivity partially but significantly. **(C) Quantification of intracellular parasite load (number of amastigotes per infected Vero cell).** Both *TcBDF6* $^{-/+}$ and *TcBDF6* $^{-/-}$ mutants showed a marked reduction in amastigote numbers. The addback strain displayed partial recovery of intracellular replication. Data represent mean ± SEM of three independent experiments. Statistical analysis was performed using one-way ANOVA followed by Tukey's test (*p<0.05, **p<0.01, ***p<0.001, ****p<0.0001 compared to WT).

After 48 hours of infection BDF6$^{-/-}$ parasites remain within the parasitophorous vacuole

As shown in Fig 5, amastigotes of the WT strain (green) are observed replicating within host cells and forming large clusters by 48 hours' p.i. In contrast, amastigotes of the *TcBDF6* $^{-/-}$ strain remain within host cells but do not exhibit significant replication. To investigate whether BDF6 KO parasites follow the classic transit of *T. cruzi* by escaping from the lysosomal-positive vacuole after host cell infection, we employed the lysosomal marker LAMP2. Notably, at 48 hours' p.i., these *TcBDF6* $^{-/-}$ amastigotes still co-localize with LAMP2 (magenta), indicating their retention within the parasitophorous vacuole. These observations suggest that BDF6 is critical for the intracellular development of *T. cruzi*, potentially by

facilitating their escape from the vacuole and supporting their subsequent replication within host cells.

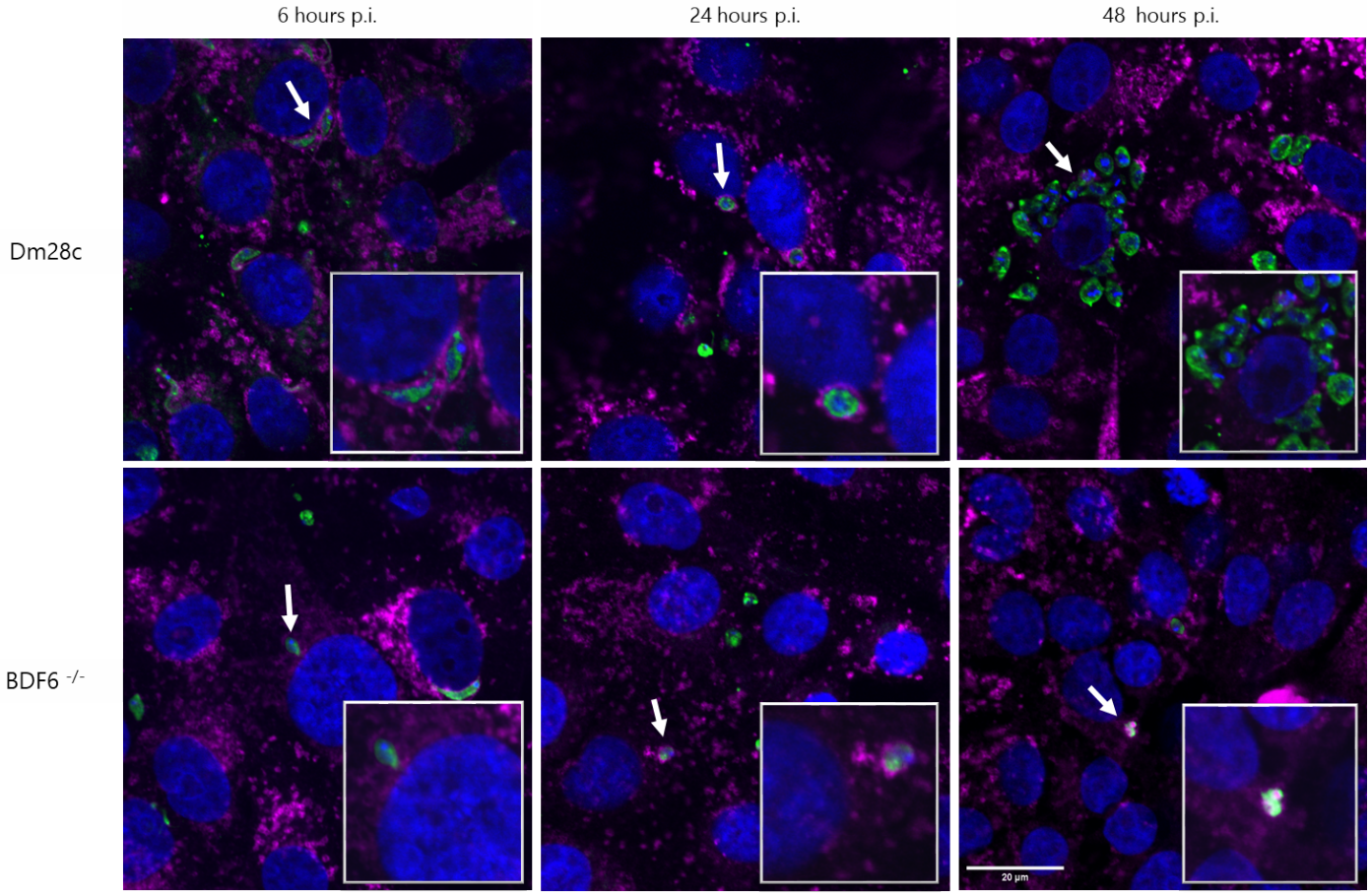

Fig 5. Immunofluorescence of infected Vero cell. Co-localization of lysosome marker and parasites were analyzed at 6, 24, and 48 hours' post-infection. DAPI (blue), a-LAMP2 (magenta) and a-Tcruzi (green). Images were captured using the ZEISS - LSM880 confocal microscope with a total magnification of 600x. Only one scale bar is shown (above right), as all the images have the same scale. Scale bar = 20um

Given that *TcBDF6* $^{-/-}$ parasites do not exit the vacuole, we hypothesized that they may be more susceptible to oxidative stress. To evaluate this, we exposed epimastigotes to different doses of H_2O_2, nifurtimox, as a source of superoxide radicals, and UV radiation. *TcBDF6* $^{-/-}$ parasites exhibited similar sensitivity to H_2O_2 and even displayed slightly greater resistance to nifurtimox compared to WT parasites (Fig 6). These results indicate that *Tc*BDF6 is not essential for resistance to oxidative stress, suggesting that the intracellular growth arrest observed is not due to an impaired ability to tolerate reactive oxygen species. Moreover, all strains showed similar sensitivity to UV irradiation, which indicates that the loss of BDF6 is not linked to defects in nucleotide excision repair mechanisms, one of the mechanisms proposed to trigger dormancy (see below). Instead, the observed growth defect probably results from an intrinsic inability to adapt to the intracellular environment, resulting in retention in the parasitophorous vacuole.

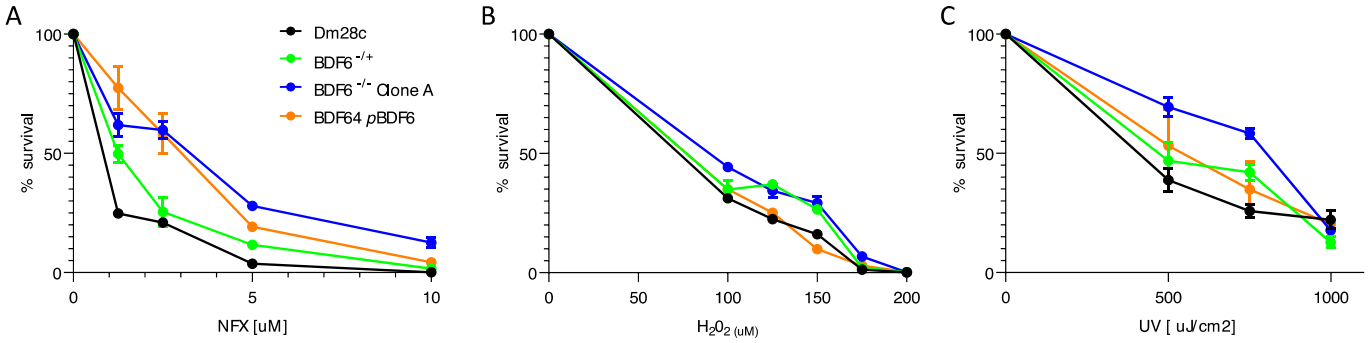

Fig 6. Sensitivity of epimastigotes to UV and oxidative stress. Epimastigotes of Dm28c WT, heterozygous (*TcBDF6* $^{-/+}$), knockout (*TcBDF6* $^{-/-}$), and addback (*TcBDF6* $^{-/-}$ pBDF6) strains were exposed to increasing doses of nifurtimox (A), H_2O_2 (B) and UV (C) and for 72 hours. Data represent mean ± SEM of four independent experiments.

*Tc*BDF6 is essential for parasite persistence *in vivo*

In vivo infection experiments performed in C57BL/6 and BALB/c nude mice revealed that *Tc*BDF6 plays a critical role in infection dynamics. The Dm28c WT strain used to generate the KO is low pathogenic, and therefore, parasitemia is typically not observed in immunocompetent C57BL/6 mice, as confirmed in our model up to day 30, before immunosuppression. However, after immunosuppression (starting at 31 d.p.i.), parasitemia rises at 50 d.p.i. in the WT strain (Fig 7.A). In contrast, mice infected with both heterozygous (*TcBDF6* $^{+/-}$) and homozygous (*TcBDF6* $^{-/-}$) mutants, as well as the add-back strain (*TcBDF6* $^{-/-}$pBDF6), failed to establish detectable parasitemia, indicating that *Tc*BDF6 is necessary to sustain a microscopically detectable bloodstream infection, even under conditions of impaired immunity (Fig. 7.B). Spleen weight, used as a surrogate marker for immune activation, was significantly increased in WT-infected and immunosuppressed animals at day 53 p.i. (Fig. 7.C), consistent with a robust inflammatory response. In contrast, spleens from mice infected with *TcBDF6* $^{-/-}$, *TcBDF6* $^{+/-}$ and the add-back strain remained similar in size to those of uninfected controls. Quantification of parasite burden in blood, heart and skeletal muscle tissues by qPCR (Fig. 7.B–E) at 53 d.p.i. showed that WT-infected mice harbored significantly higher parasite loads compared to *TcBDF6* $^{-/-}$ infected animals, where parasites were almost undetectable. The add-back strain partially restored tissue colonization at levels similar to or even higher than the heterozygous strain. Despite differences in parasitemia levels, mice infected with WT, heterozygous, or add-back strains and treated with cyclophosphamide showed a residual and comparable humoral response against *T. cruzi* antigens, as indicated by similar levels of specific IgG that persisted after 53 d.p.i. In contrast, mice infected with the homozygous KO strain exhibited IgG levels comparable to those of uninfected controls, which—as expected—did not develop a specific antibody response (S3 Fig).

To further assess the role of *Tc*BDF6 in the absence of adaptive immunity, infections were also performed in nude mice. Nude mice lack mature T lymphocytes, resulting in a severely impaired adaptive immune response. While they retain functional B cells and innate immune components, their ability to mount effective cell-mediated immunity is profoundly compromised. In this model, wild-type parasites reached high parasitemia levels starting around 9 d.p.i. (Fig 7.F). *TcBDF6* $^{-/-}$ mutants again failed to establish parasitemia in nude mice, while those infected with the add-back strain showed partial recovery, confirming the requirement of *Tc*BDF6 for effective replication and systemic infection, even in

immunodeficient hosts. Quantification of parasite burden in blood, heart, and skeletal muscle tissues by qPCR (Fig 7. G, I–J) showed that WT-infected nude mice harbored significantly higher parasite loads compared to *TcBDF6* $^{-/-}$ -infected animals, where the parasites were undetectable. The add-back strain partially restored tissue colonization but with, in this case, parasite levels lower than those observed for the heterozygous strains. In nude mice, splenomegaly was evident in WT-, heterozygous- and add-back-strain infected animals (Fig 7.H). In contrast, spleens from nude mice infected with *TcBDF6* $^{-/-}$ remained similar in weight to those of uninfected controls, indicating that *TcBDF6* $^{-/-}$ mutants consistently failed to establish infection, even in the absence of T cell-mediated immune, highlighting the essential role of *Tc*BDF6 for intracellular development.

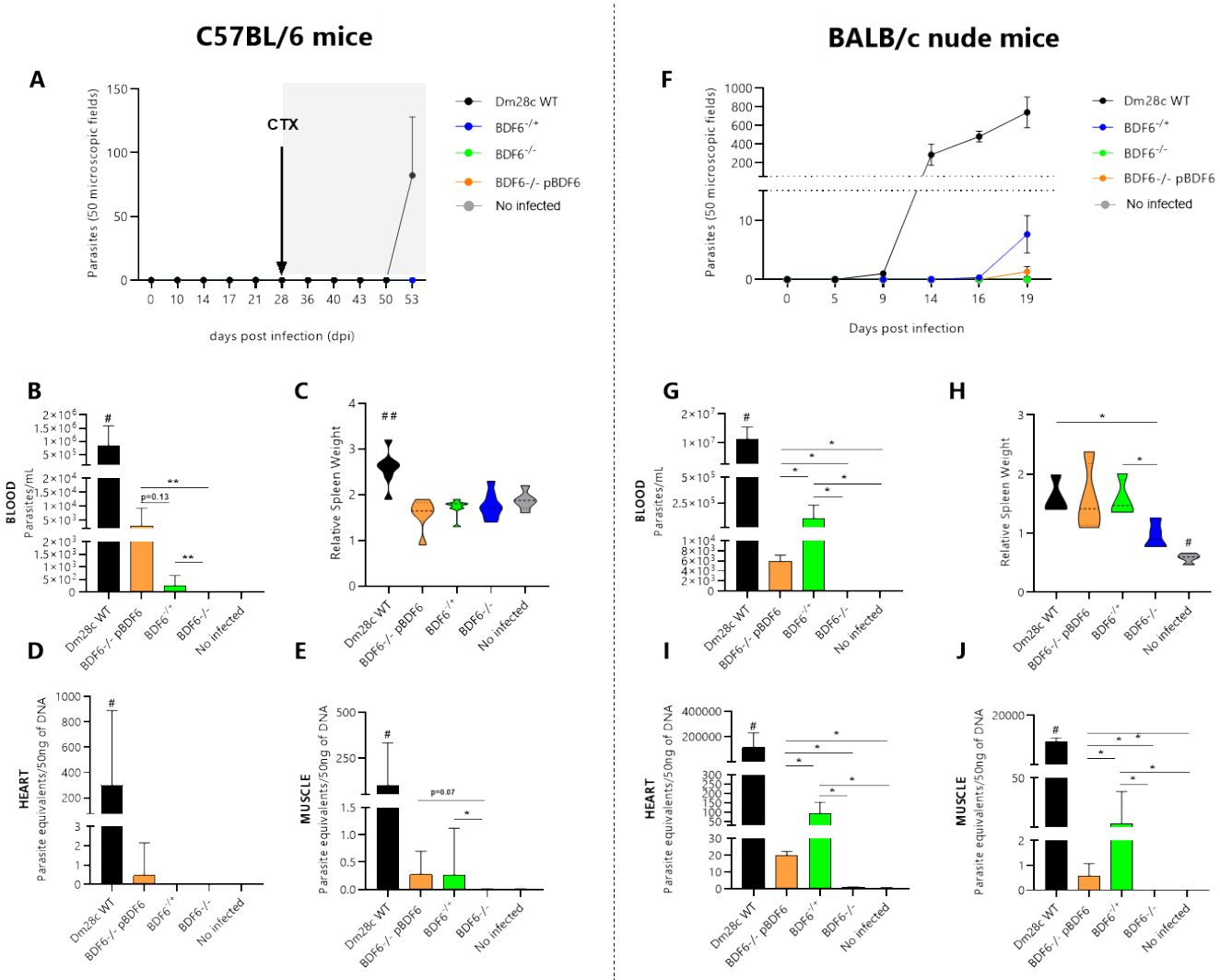

Fig 7. *In vivo* infections. (A–E) Infections in immunocompetent C57BL/6 mice subjected to immunosuppression with cyclophosphamide (CTX). (A) Parasitemia was assessed by direct blood examination at multiple time points post-infection. Only wild-type (Dm28c) parasites exhibited detectable parasitemia following immunosuppression. **(B)** Quantification of parasite load in blood by qPCR revealed a significant reduction in *TcBDF6*$^{-/-}$ mutants compared to WT, while the add-back strain (*TcBDF6*$^{-/-}$pBDF6) showed partial restoration. **(C)** Relative spleen weight, used as an indicator of immune activation, was significantly elevated in WT-infected mice but not in those infected with *TcBDF6* $^{-/-}$ mutants or the add-back strain. **(D, E)** Parasite load in heart and muscle tissues, measured by qPCR, was markedly decreased in *TcBDF6*$^{-/-}$ infected mice, with partial recovery in the add-back group. **(F–J) Infections in immunodeficient BALB/c NUDE mice**, **which lack functional T cells. (F)** Parasitemia kinetics showed robust parasite proliferation in WT-infected nude mice, while *TcBDF6* $^{-/-}$ mutants failed to establish significant parasitemia. Complementation

partially restored parasitemia levels. **(G)** qPCR quantification in blood confirmed significantly reduced parasite levels in *TcBDF6* $^{-/-}$-infected BALB/c nude mice, with partial restoration in the add-back strain. **(H)** Relative spleen weights remained low in *TcBDF6* $^{-/-}$ infected mice, comparable to uninfected controls, suggesting reduced immune activation. **(I, J)** Parasite burden in heart and muscle tissues was significantly reduced in *TcBDF6* $^{-/-}$ infected nude mice, with partial restoration upon complementation. Data are expressed as median ± range and were analyzed using non-parametric tests (Kruskal-Wallis followed by Mann-Whitney U test). Results represent two independent experiments with 3–5 animals per group. Statistical comparisons between groups were performed using non-parametric tests. Significance levels are indicated as follows: *$p < 0.05$, **$p < 0.01$, ***$p < 0.001$ (between specified groups); #$p < 0.05$, ##$p < 0.01$ versus all other groups. Fig 7E and 7B show a marked difference in p-values. While one comparison reaches statistical significance ($p < 0.05$), the other shows a trend toward significance ($p = 0.07$), suggesting a potential biological effect despite not meeting conventional thresholds. Notably, the comparison appears different visually but is not statistically significant.

Discussion

Understanding how chromatin-associated proteins regulate the complex life cycle of *T. cruzi* remains a major challenge. In this study, we used the CRISPR/Cas9 system, a powerful genetic tool, to investigate the biological functions of the *Tc*BDF6 protein. A key limitation of gene knockout approaches is the inability to generate viable epimastigotes if the target gene is essential across all life stages. In such cases, complete gene disruption may not be feasible. Even when homozygous KOs are obtained, the resulting phenotypes can range from severe growth defects to subtle or undetectable changes. For instance, ablation of the mitochondrial calcium uniporter b (*Tc*MCUb) results in epimastigotes with a significant growth defect, reduced respiration and metacyclogenesis rates, and markedly diminished infectivity [25]. Similarly, deletion of the pleiomorphic protein P21 gene leads to epimastigotes with reduced growth and can still differentiate into metacyclic trypomastigotes, however, they are less infective [26] . Deletion of Topoisomerase 3α (*Tc*Topo3α) reduces to half the infectivity and intracellular amastigote development. *Tc*Topo3α KO epimastigotes grow nearly normally, but they are highly sensitive to gamma radiation and various drugs that induce replication stress [27]. In other instances, heterozygous mutants, carrying only a single functional gene copy, exhibit significant phenotypes and are useful models to infer the gene's function and significance. A clear example is the *Tc*NTPDase-1 gene (Ecto-Nucleoside Triphosphate Diphosphohydrolase 1), hemizygous mutants for this gene grow normally as epimastigotes but are less infective and show impaired intracellular development [28]. However, there are a few cases in which the phenotype is primarily manifested during the life cycle stages that occur in the mammalian host. The disruption of active trans-sialidase genes, which does not affect the parasite's ability to grow as epimastigotes or differentiate into metacyclic trypomastigotes. These parasites can still invade host cells and escape from the parasitophorous vacuole. However, they exhibit impaired differentiation of amastigotes into trypomastigotes, and parasites do not egress from the host cell [29]**.** Another example is presented in this study.

Deletion of the *TcBDF6* gene results in an exceptionally interesting and unique phenotype, unlike any previously described. Remarkably, while *TcBDF6* KO parasites proliferate almost normally as epimastigotes and can differentiate into metacyclic trypomastigotes, they are unable to infect efficiently and replicate as amastigotes once inside host cells, highlighting a life stage–specific essentiality not previously described for any BDF in this parasite.

We previously demonstrated that *Tc*BDF6 is part of a TINTIN-like complex, an autonomous subcomplex of the yeast chromatin remodeling complex NuA4 (known as TIP60 in humans). In *T. brucei*, putative orthologs of this complex were identified using immunoprecipitation [30]. Using a proximity labeling approach, we also identified structural orthologs of different chromatin remodeling complexes, including several NuA4 components, clearly indicating the presence of a NuA4-like complex in trypanosomatids (Rodriguez Araya, personal

communication).

Although the full range of its functions remains to be elucidated, NuA4 is a key nuclear complex involved in numerous processes directly or indirectly associated with chromatin structure. In yeast, it contains the only essential acetyltransferase [31]**.** In both yeast and mammals, NuA4/TIP60 plays a central role in transcriptional regulation, primarily through histone [18]. It has also been implicated in cell cycle progression and DNA repair [32,33]**.**

A possible explanation for the phenotype of *TcBDF6*$^{-/-}$ parasites is that they have a higher predisposition to be in a dormant state. Dormancy is defined as the ability to enter a quiescent state with reduced metabolic activity and no replication [34,35]**.** These dormant parasites can survive under stressful environmental conditions, such as drug treatment, resulting in the persistence of the infection [36]**.** Although this phenomenon was first described in intracellular amastigotes, where it is relevant for infection persistence, it has also been observed in epimastigotes [27]**.**

The transition into and out of dormancy in *T. cruzi* is thought to be a spontaneous and stochastic process, and the mechanisms driving dormancy remain unknown [37]. The only established mechanistic hypothesis suggests that spontaneous DNA damage activates DNA repair mechanisms, leading to cell cycle arrest until the repair is complete [24,27]. Since NuA4 has been associated with DNA repair, it is plausible that the phenotype observed in *TcBDF6*$^{-/-}$ parasites could be linked to dormancy. However, the dormancy hypothesis does not fully explain this phenotype. While a higher number of dormant epimastigotes is observed, it doesn`t explain the increased average doubling time. This increase in the doubling time is more likely associated with a general slowing of the G0/G1 phase progression, which may also explain the reduced average size of the parasites. Furthermore, amastigotes do not appear to "awaken" from the dormant state after 11 days in Vero cells, nor after more than 20 days in immunosuppressed nude mice. Finally, the observation that that *TcBDF6*$^{-/-}$ parasites do not show increased susceptibility to reactive oxygen species or UV irradiation compared to the parental strain argues against the hypothesis that amastigotes are in a dormant at least triggered by DNA damage.

As mentioned above, the *Tc*TINTIN complex is structurally similar to a subcomplex of NuA4/TIP60 yeast and human complexes. This structural conservation indicates that, even without evident sequence similarity, *Tc*BDF6 and Eaf7 and BRD8 could be considered functional orthologs [16]**.** The deletion mutant of Eaf7 exhibits strong growth deficiencies at 37 °C but grows normally at 30 °C [38]**.** As well as *tcbdf6*, deletion of *eaf7* also does not generate sensitivity to DNA-damaging agents as does the elimination of other NuA4 components. Mutagenesis experiments indicate that the Eaf5/7/3 (TINTIN) complex is involved in the transcription of specific genes, playing a role in nucleosome dynamics during transcription elongation by promoting nucleosome destabilization ahead of the polymerase. On the other hand, BRD8 KO in mice leads to preweaning lethality, and its dysregulation has been associated with various cancers [39]**.** Interestingly, in both lung epithelial and colorectal cancer cells, BRD8 has been directly linked to the regulation of cell cycle genes, likely in a TIP60-independent manner [40]. These observations highlight the multifunctional nature of BRD8 in mammalian cells and raise the question of whether *Tc*BDF6 might similarly participate in diverse nuclear processes beyond its association with the *Tc*TINTIN complex.

Although the precise cause of the observed phenotype lies beyond the scope of this study

and requires further investigation, we speculate that the effects of *Tc*BDF6 absence on MT trypomastigotes infectivity and amastigote proliferation may arise from distinct mechanisms. Metabolic or genetic defects affecting core functions are unlikely, as such alterations would have severely impacted epimastigote growth, which we found to be only mildly affected. Furthermore, the differentiation from MT trypomastigotes to amastigotes appears to proceed normally. Infectivity and escape from the endocytic vacuole—processes largely driven by surface proteins—may be selectively impaired in the absence of *Tc*BDF6. In contrast, the arrest in intracellular amastigote replication, which does not result from increased sensitivity to oxidative stress, might instead reflect defects in stage-specific energy metabolism or cell cycle control. While the underlying mechanisms remain to be elucidated, our findings support the idea that these processes are epigenetically regulated and critical for successful amastigote development. Future proteomic and transcriptomic analyses can provide valuable insights into *Tc*BDF6 function. Proteomic approaches may help identify interaction partners, including chromatin-associated complexes or histone-modifying enzymes. In parallel, transcriptomic analysis can uncover gene expression changes resulting from the loss expression of the protein. Together, these strategies can contribute to defining the role of *Tc*BDF6 in the *T. cruzi* life cycle, particularly in processes that may be required for successful interaction with the mammalian host.

The findings presented here open promising avenues for future research with potential implications for Chagas disease treatment and prevention. Previously, we demonstrated that inhibitors of BET family BDs exhibit trypanocidal activity. Among the eight *T. cruzi* BDFs, *Tc*BDF1 and *Tc*BDF3 are candidates for classification within this family. To date, *Tc*BDF6 has not been assigned to any known BD family. However, its involvement in an evolutionarily conserved complex related to NuA4/TIP60 suggests a possible functional relationship with BRD8. BRD8, along with BAZ1B, BRWD1, BRWD3, CREBBP, EP300, PHIP, and WDR9, belongs to subgroup III of human bromodomain-containing proteins [41]**.** The development of specific inhibitors targeting BRD8 is relatively recent and less advanced than BET family inhibitors (group II), and their efficacy against *T. cruzi* has not yet been explored. It is noteworthy that *Tc*BDF6 is essential for intracellular amastigote development—an ideal point of intervention for designing new trypanocidal therapies. Additionally, a highly attenuated *T. cruzi* strain, like *TcBDF6* $^{-/-}$, that grows efficiently as epimastigotes and differentiates into trypomastigotes, yet fails to maintain infection, could serve as a potential vaccine candidate for immunizing domestic animals involved in the maintenance of the domiciliary and peridomiciliary transmission cycles of *T. cruzi*.

Materials and methods

Parasite Cultures. *T. cruzi* Dm28c epimastigotes were cultured at 28°C in LIT medium (5g/L liver infusion, 5g/L bacto-tryptose, 68mM NaCl, 5.3mM KCl, 22 mM Na_2HPO4, 0.2% (w/v) glucose, and 0.002% (w/v) hemin) supplemented with 10% (v/v) fetal calf serum (FCS) (Internegocios S.A., Argentina).

***TcBDF6* KO Lines Generation.** To knockout the *TcBDF6* gene, CRISPR/Cas9-mediated genome editing was done, as previously described [42,43]. Briefly, the Cas9/pTREX-n vector (Addgene, catalog number: 68708) was used to clone a specific sgRNA sequence to target *TcBDF6* gene (TriTrypDB ID: *Tc*C4B63_41g80), which encodes the BDF6 protein. The sgRNA carrying the specific protospacer sequence was amplified from the pUC_sgRNA plasmid using the oligonucleotides sgRNAFw and sgRNARv (S1 table) and cloned into Cas9/pTREX-

n plasmid. Donor DNA was generated by PCR using the blasticidin-S deaminase gene (*Bsd*) as template. Ultramers used were *TcBDF6*_BSD_KO and *TcBDF6*_BSD_KO Reverse (S1 table) and included the homology region for DNA recombination. *T. cruzi* DM28c epimastigotes were co-transfected with donor DNA and Cas9/pTREX-n plasmid, and mutant parasites (*TcBDF6* $^{-/-}$) were selected by adding G418 (250 µg/mL) and Blasticidin (5 µg/mL) to the culture medium, ensuring continuous CRISPR-Cas9 system operation.

Subsequently, limiting dilution cloning assays were performed. Mutant genotypes were confirmed by PCR using Val_BDF6_KO_Fw and Val_BDF6_KO_Rv oligonucleotides (S1 table). PCR product for Dm28c WT strains showed one band of 1391 bp, while homozygous (*TcBDF6* $^{-/-}$) mutant strains displayed one band of 1791 bp, and heterozygous (*TcBDF6* $^{-/+}$) strains showed both bands. This result was interpreted as a successful homologous recombination of the *Blasticidin* resistance gene into the *TcBDF6* gene locus. Three clones were selected, one heterozygous (*TcBDF6* $^{-/+}$), and two homozygous, named *TcBDF6* $^{-/-}$ Clone A and *TcBDF6* $^{-/-}$ Clone B.

Complementation of KO strains. *TcBDF6* gene was amplified from genomic DNA (gDNA) extracted from wild-type *T. cruzi* Dm28c epimastigotes. PCR amplification employed a forward oligonucleotid *TcBDF6* MutCas9 (S1 table) designed to introduce silent mutations in the Cas9 recognition site at the 5′ region of the *TcBDF6* gene, by modifying the third bases of the first six codons and introduced a *Bam*HI restriction site upstream of the gene. These mutations preserve the amino acid sequence but prevent recognition by the CRISPR-Cas9 system in KO strains. The reverse oligonucleotid *TcBDF6 Eco*RV (S1 table) bound to the 3′ regions of the gene and introduced an *Eco*RV restriction site. The PCR products and the pENTR3C vector were digested with *Bam*HI and *Eco*RV restriction enzymes, resolved on a 1% agarose gel, and purified using the Wizard® SV Gel and PCR Clean-Up System (Promega). The purified fragments were ligated and transformed into *E. coli* DH5α cells. Plasmid pENTR3C-BDF6-mc9 was isolated.

We transferred *TcBDF6* from the entry vector (*pENTR3C*-BDF6-mc9) into the destination vector *pTEX-GW*, shearing Hygromycin resistance by LR recombination reaction using Clonase® enzyme mix (Invitrogen). *pTEX-GW* was linearized with *Eco*RI (Promega) for 4 hours at 37°C to enhance recombination efficiency. The resulting construct was transformed into *E. coli*, purified, and subsequently used for transfection into *T. cruzi* to complement mutant strains and study *Tc*BDF6 function.

Growth Curves. An initial inoculum of $5x10^6$ epimastigotes/ml was cultured in LIT medium supplemented with 10% FBS, 0.8% glucose, and 0.002% hemin. Daily, aliquots of the culture were taken, and diluted in a 4% PBS-formaldehyde solution. Parasites were counted by Neubauer chamber or hematological counter (Wiener Lab Counter 19) in the white cells channel.

Dormancy Assay. Dormancy assays were performed as described by [24]. Briefly, epimastigotes in the exponential growth phase were harvested and washed twice with 1X PBS. Parasites were suspended in 1 mL of PBS containing 1 µL of CFSE (CellTrace CFSE, Thermo Fisher) stock solution. After 20 minutes of incubation in the dark at 28°C, the reaction was stopped adding 200 µL of FBS, followed by centrifugation at 3500 × g for 10 minutes. Parasites were suspended in LIT medium supplemented at a final concentration of 5×10^6 parasites/mL. To assess fluorescence intensity at different time points, samples of approximately 1×10^6 parasites were collected daily from day 1 (24 hours) till day 6 (144 hours). Samples were centrifuged, washed with 1X PBS, and fixed for 15 minutes with 50 µL of 4% filtered paraformaldehyde (PFA), centrifuged, and suspended in 1X PBS for analysis.

Ten thousand events per sample were acquired using BD FACSAriaII (BD Biosciences). The percentage of dormant epimastigotes was calculated by counting the burden of parasites after 144 hs retaining maximum fluorescence intensity, which was previously determined by the intensity of fluorescence in parasites at 24 hours. The results were analyzed using FlowJo software (Bd Biosciences).

Quantification of the size of epimastigotes. Fixed epimastigotes from exponential stage were mounted on microscope slides and stained with Giemsa solution, in a dilution 10% (v/v), for 20 minutes. Bright-field microscopy images were captured at 40× magnification and saved in TIFF format to preserve quality for analysis. Image analysis was performed using the ImageJ software (version 1.54p). Images were converted to grayscale (Image > Type > 8-bit) to facilitate segmentation. A threshold was applied (Image > Adjust > Threshold) to clearly distinguish epimastigotes from the background. The threshold settings were adjusted to ensure precise delineation of the parasite boundaries. Subsequently, the areas corresponding to epimastigotes were selected using the Analyze Particles function (Analyze > Analyze Particles). Parameters for particle size and circularity were set to filter out noise and exclude non-epimastigote structures. Only objects matching the expected morphology and size of epimastigotes were included in the analysis. For each selected epimastigote, measurements of individual cell areas were generated by ImageJ (version 1.54p).

Ultra Resolution-Expansion microscopy. To visualize morphological characteristics of epimastigotes and metacyclic trypomastigotes, the methodology described by **[44]** was used. Briefly, one million parasites were washed with PBS, settled on poly-D-lysine-coated coverslips, and fixed with 4% formaldehyde and acrylamide. Gelation was performed using a monomer solution, followed by polymerization on ice and incubation at 37 °C. The gels were detached using a denaturation buffer and then incubated at 95 °C for 1.5 hours. After expansion in Milli-Q water overnight, gels were washed in PBS, stained with DAPI/NHSester Alexa Fluor 647 (Thermo Fisher Scientific, Carlsbad, CA, USA) overnight at 4 °C, and subjected to a second round of expansion with multiple water exchanges. Images were acquired with a confocal Zeiss LSM880 microscope. ImageJ software was used to pseudocoloring and processing all images **[45]**.

Cell Cycle Analysis of epimastigotes by Flow Cytometry. To determine cell cycle distribution in *T. cruzi* epimastigotes, we performed flow cytometric analysis based on DNA content using propidium iodide (PI) staining. Briefly, epimastigotes from exponential phase cultures were collected, washed twice with PBS, and fixed in cold 70% ethanol and incubated on ice for 40 minutes to ensure optimal fixation and permeabilization. Cells were centrifuged at 3,000 × g for 10 minutes and washed twice with PBS to remove residual ethanol. The pellet was then resuspended in PI staining solution (50 µg/mL PI, 100 µg/mL RNase A, and 0.1% Triton X-100 in PBS). Samples were incubated for 30 minutes at 37 °C in the dark. Stained cells were analyzed on a BD FACSAriaII cytometer (BD Biosciences) equipped with a 488 nm laser. PI fluorescence was collected in the FL2 channel (585/42 nm filter). A total of 10,000 events per sample were recorded and cell cycle distribution was determined using FlowJo software (Version 10). Debris and aggregates were excluded by appropriate gating, and the percentage of cells in G_0/G_1, S, and G_2/M phases was calculated based on DNA content histograms.

Oxidative and UV stress assays. To evaluate the response of epimastigotes to oxidative stress, parasites in exponential growth phase were collected (5×10^6 parasites/mL),

centrifuged at 4,000 × g for 10 minutes, and washed twice with 1× PBS to eliminate residual culture medium. For hydrogen peroxide (H_2O_2) treatment, parasites were incubated for 30 minutes in PBS containing 0, 50, 100, or 150 μM H_2O_2, then washed, suspended in LIT medium (5 × 10^6 parasites/mL), and plated in triplicate (500 μL/well) in 24-well plates. For drug-induced oxidative stress, 500 μL of epimastigotes (10×10^6 parasites/mL) from WT, *TcBDF6* $^{-/+}$, and *TcBDF6* $^{-/-}$ lines were seeded in triplicate and treated for 72 hours at 28 °C with increasing concentrations of benznidazole or nifurtimox. For UV-induced stress, parasites were exposed to increasing doses of UV radiation (500, 750, and 1000 μJ/cm^2), then resuspended in LIT medium and incubated for 72 hours. After treatment, parasites were fixed with 3.7% formaldehyde and counted using a Neubauer chamber to determine % survival.

***In vitro* Metacyclogenesis.** Metacyclogenesis of all strains was evaluated as described by **[46]**. Briefly, cultures in exponential phase with an initial concentration of 5x10^6 epimastigotes/ml, parasites were incubated at 28°C in 24-well plates, in quadruplicate, with 500 µl of LIT medium (0.8 % glucose) at pH 6 for 7 days. Subsequently, aliquots of the culture were taken and diluted in a 4% PBS-formaldehyde solution, and the different parasite stages were counted in a Neubauer chamber. To determine the percentage of metacyclogenesis, the number of trypomastigotes was counted and expressed as a proportion of the total number of parasites.

***In vitro* infection of Vero Cells.** Vero cell line (ATCC CCL-81) was cultured in DMEM (Dulbecco's Modified Eagle's Medium powder, Gibco™, Thermo Fisher Scientific, Cat. No. 12100-046), supplemented with 10% (v/v) heat-inactivated FBS, at 5% CO_2, at 37°C. Metacyclic trypomastigotes (MT) were obtained as previously mentioned and quantified. Then, in 24-well plates containing 12-mm round glass coverslips, 20,000 Vero cells were seeded per well in DMEM supplemented with 2% FBS and incubated for 24 hours at 37°C, 5% CO_2. Cells were infected with MT at a multiplicity of infection (MOI) of 10:1. After 16 hours of incubation (ON), non-adherent parasites were removed by washing twice with PBS 1X, and the DMEM medium was replaced. Cultures were maintained by five days, infected cells were washed twice with PBS and fixed with PFA 4%. Parasites were visualized by Giemsa or DAPI staining and immunostaining using mouse *a-T. cruzi* antibody. Images were acquired with a Zeiss LSM 880 confocal microscope. Microphotographs were taken, and the percentage of infected cells and the mean number of intracellular amastigotes per infected cell were quantified. Three hundred cells from each quadruplet were evaluated, and the experiment was repeated three times.

Colocalization of amastigotes and lysosomal markers. Colocalization assay was performed using antibodies against the endogenous lysosomal protein LAMP2 and a mouse *a-T. cruzi* antibody **[47]**. Infections were performed as previously described. For lysosomal detection, cells were incubated overnight at 4°C with a primary anti-LAMP2 antibody diluted in 1% PBS-BSA. Samples were washed three times with PBS and subsequently incubated for 1 hour at room temperature, protected from light, and stained with an Alexa 555-conjugated secondary antibody. A second immunostaining step was performed using a primary anti-*T. cruzi* antibody followed by a FITC-conjugated secondary antibody to detect amastigotes. After three final PBS washes, samples were mounted with a DAPI-containing medium to stain the nuclei of both Vero cells and amastigotes [48,49]. Coverslips were placed on the samples and sealed. Images were acquired by confocal microscopy. Colocalization of LAMP2 (lysosomes) and anti-*T. cruzi* signals were analyzed to evaluate the retention of amastigotes within the parasitophorous vacuole.

Mice infections. The infection experiments were performed on C57BL/6 male mice (6–8 weeks old) and on Balb/c male nude mice (6–8 weeks old, immunodeficient, lacking T cells). Animals were housed in HEPA-ventilated racks with *ad libitum* access to food and water. All procedures were conducted by institutional and national ethical guidelines for animal care and use. The protocol was approved by the ethical committee for animal experiments (CICUAL) of the Facultad de Ciencias Médicas at the Universidad Nacional de Rosario (Res N° 911/2023).

Mice were divided into five experimental groups (n=3-6/group), each named according to the *T. cruzi* strain used for infection: Uninfected control (negative control), Dm28c WT strain (positive control strain), *TcBDF6* $^{-/+}$ (hemizygotes strain), *TcBDF6* $^{-/-}$ (KO strain) and *TcBDF6* $^{-/-}$*pBDF6* (add-back strain). For the infection, MT were obtained as described above. One million MT per mouse were injected intraperitoneally in PBS+Glucose (100 mg/dL). Control group received the same amount of vehicle. The experiment was conducted over 53 days for C57BL/6 mice and 21 days for Balb/c nude mice, monitoring parasitemia regularly post-infection (pi).

Blood parasite burden. Parasitemia was assessed by quantifying circulating trypomastigotes in peripheral blood samples obtained via tail vein puncture using heparinized tips. Fresh blood samples were mounted directly onto microscope slides without fixation or staining and examined immediately under a light microscope. Trypomastigotes were counted in a defined volume of blood to estimate parasite burden as previously reported [50].

C57BL/6 mice immunosuppression. Dm28c WT, *TcBDF6* $^{-/+}$, *TcBDF6* $^{-/-}$ and *TcBDF6* $^{-/-}$ *pBDF6* -infected C57BL/6 mice (n=3-6/group) were treated with three doses of cyclophosphamide (200 mg/kg, IP), administered every four days, starting on day 31 post-infection, to induce immunosuppression during the course of infection. An uninfected group of mice (n=4) was subject to the same procedure.

Detection of Parasite Burden in tissues. Hearts and skeletal muscles were collected and stored at -80°C for subsequent DNA extraction, following the method previously described **[51]**. Briefly, total DNA was extracted from each sample after tissue disaggregation with a lysis buffer (10 mM Tris-HCl; 0.1 M NaCl; 10 Mm EDTA; 0.5% SDS, 300 µg/mL proteinase K from Inbio Highway®. pH = 7.6). The samples were then heated for 2 h at 55 °C, and extracted twice with a phenol–chloroform–isoamyl alcohol mixture (25:24:1) (Sigma Chemical Co., St. Louis, MO, USA). Cold ethanol (AAPER Alcohol and Chemical Co., Shelbyville, KY, USA), twice the volume of the extracted sample, was then added and the samples were placed at −80 °C for ON. Samples were centrifuged for 30 min at 8000g and washed with 70% ethanol, vacuum dried, and then resuspended in 100 µL of sterile miliQ water. DNA samples were adjusted to a final concentration of 25 ng/µL and were used as a template for the qPCR reactions using the specific oligonucleotides for *T. cruzi*: TCZ-F and TCZ-R (S1 Table), which recognize a satellite sequence of 182 bp present in the parasite genome. To generate the *T. cruzi* quantification curve, 25 mg of uninfected mouse hearts or muscles were mixed with $1x10^6$ trypomastigotes. Total DNA was extracted, and the final concentration was adjusted to 25 ng/ml. Following, the standard curves were constructed by serial dilutions using DNA from uninfected tissues (25 ng/ml) as diluent. PCR reactions were performed using a HOT FIREPol EvaGreen qPCR Mix Plus kit (Solis Biodyne®) with a StepOneTM Real-Time PCR Systems (Applied Biosystems®) instrument. The PCR conditions consisted of an initial denaturation at 95 °C for 10 min, followed by 40 cycles of 95 °C for 10 s, 50 °C for 15 s, and 72°C for 15 s, with fluorescence acquisition at 81°C for 15 s.

Amplification was immediately followed by a melt program with an initial denaturation of 10 seconds at 95°C, 60°C for 20 seconds, and then a stepwise temperature increase of 1 °C/s to 90°C. The parasite load was expressed as equivalent parasites in 50 ng of murine DNA.

qPCR quantification of parasite load in blood. Blood samples were immediately mixed with two volumes of lysis buffer containing 6M guanidine hydrochloride (Sigma®) and 200 mM EDTA, pH 8.0 (GE buffer). A pGEM-T plasmid (Promega®) was used as a heterologous internal standard (IS) and all samples were mixed before DNA purification with 1 pg of the IS. DNA was purified with High Pure PCR Template Preparation Kit (Roche®) following the manufacturer's instructions. PCR was performed as already mentioned. A quantification curve for *T. cruzi* was generated by spiking uninfected mouse blood with 1×10^6 Tulahuen strain trypomastigotes or 1000 pg of IS DNA, followed by immediate processing as described. Total DNA was extracted, and both standard curves were constructed by serial dilutions using uninfected mouse blood DNA as diluent. The parasite load was expressed as number of *T. cruzi*/ml of blood as described in [52].

ELISA for Anti-*T. cruzi* Antibody Detection. Blood samples were collected at day 53 p.i. by cardiac-punction with anticoagulant and plasma was obtained by centrifuging at 5000 rpm and stored at −20°C until analysis. ELISA microplates coated with *T. cruzi* lysate (Wiener Lab®) were used. Plasma samples were diluted 1:32 in 0.5% BSA and incubated in duplicate for 1 hour at 37°C. Specific anti-*T. cruzi* antibodies were detected using a peroxidase-conjugated goat anti-mouse IgG antibody (diluted 1:2000; Sigma®), incubated for 1 hour at 37°C. After washing, TMB substrate was added, and the reaction was stopped with sulfuric acid. Absorbance was measured at 450 nm with correction at 545 nm in an ELISA reader (Epoch Biotek Instruments®).

Statistical analysis

Statistical analysis was performed with GraphPad Prism 3.0 software (GraphPad Software, La Jolla, CA, USA). For in vitro experiments, comparisons were made using One-Way Analysis of Variance (ANOVA) followed by Tukey's post hoc test. For in vivo experiments in mice, non-parametric tests were used: Kruskal-Wallis followed by Mann-Whitney U test. Depending on the variable analyzed, data are expressed as mean ± standard error of the mean (SEM) or median ± range. Results represent one of three independent experiments performed on different days using different culture batches. At least 3 biological replicates per experimental group were used in each experimental round. Significance was set at $p<0.05$.

Supporting information

S1 Table. Description of the oligonucleotides. Oligonucleotides and ultramers used for the generation of the *TcBDF6* knockout line. The table lists the sequences of single guide RNAs (sgRNAs), primers for PCR validation, and constructs used for CRISPR/Cas9 mediated gene editing. The *Tc*BDF6_MutCas9 primer contains homology regions flanking the Cas9-induced cleavage site. The ultramers correspond to long single-stranded oligonucleotides used for homologous recombination and insertion of the blasticidin resistance gene (BSD) at the *TcBDF6* locus.

S1 Fig. Genotyping of *T. cruzi* mutant strains by PCR. PCR amplification was performed using oligonucleotides flanking the insertion site of the blasticidin resistance cassette

(Val_KO_BDF6_Dm28c oligonucleotides). The wild-type Dm28c strain shows a single band of 1391 bp, corresponding to the endogenous *TcBDF6* allele. The heterozygous *TcBDF6* $^{-/+}$ line shows two bands 1391bp and 1700 bp, corresponding to the disrupted allele with the resistance cassette. The homozygous *TcBDF6* $^{-}/^{-}$ clones (Clone A and Clone B) display the single band of 1700 bp. The add-back strain *TcBDF6* $^{-/-}$pBDF6 shows the same pattern as the homozygous knockouts, confirming that complementation was performed in the *TcBDF6* $^{-/-}$ background.

S2 Fig. Deletion of *TcBDF6* enhances *T. cruzi* metacyclogenesis. Percentage of metacyclic trypomastigotes formed during in vitro metacyclogenesis was quantified in WT, *TcBDF6* $^{-/+}$ heterozygous, *TcBDF6* $^{-/-}$ knockout clones (A and B), and addback strain *TcBDF6* $^{-/-}$pBDF6. Data represent mean ± SD of three independent experiments.

S3 Fig. Anti-*T. cruzi* IgG response. Serum IgG levels were measured by ELISA at 53 days p.i. in C57BL/6 mice infected with metacyclic trypomastigotes Dm28c WT, *TcBDF6* $^{-/+}$, *TcBDF6* $^{-/-}$, or the add-back strain *TcBDF6* $^{-/-}$pBDF6 and treated from day 31 onwards with 3 doses of cyclophosphamide. A group of uninfected animals subject to the same protocol was included as a negative control. Bars represent mean ± SD). Results represent two independent experiments with 3–5 animals per group. Statistical comparisons between groups were performed using non-parametric tests. Significance levels are indicated as follows: *$p < 0.05$, **$p < 0.01$, ***$p < 0.001$ (between specified groups); #$p < 0.05$, ##$p < 0.01$ versus all other groups.

Acknowledgments

We would like to thank Rodrigo Vena for technical confocal microscope assistance, Dolores Campos for Vero Cells technical assistance and Mara Ojeda for technical assistance with flow cytometry. We also wish to express our gratitude to the Wiener Lab for their contribution of ELISA reagents.

Author Contributions

Conceptualization: Ana Rosa Perez, Roberto Docampo, Patricia S. Romano, Victoria Boselli, Esteban C. Serra.
Data curation: Victoria Boselli, Esteban C. Serra
Formal analysis: Victoria Boselli, Virginia G. Perdomo, Florencia Pacini,
Funding acquisition: Esteban C. Serra
Investigation: Victoria Boselli, Florencia Pacini, Juan A. Cueto, Alejandro Pezza., Virginia G. Perdomo.
Methodology: Victoria Boselli, Virginia G. Perdomo, Florencia Pacini, Juan A. Cueto, Alejandro Pezza.
Project administration: Esteban C. Serra.
Writing – Original Draft Preparation: Victoria Boselli, Virginia G. Perdomo, Esteban C. Serra.
Writing – Review & Editing: Victoria Boselli, Esteban C. Serra, Ana Rosa Perez, Roberto Docampo, Patricia S. Romano.

References

1. PAHO / WHO - Chagas disease. 16 Jul 2025. Available: https://www.paho.org/en/topics/chagas-disease#3

2. Coura JR, Viñas PA. Chagas disease: a new worldwide challenge. Nature. 2010;465: S6–S7. doi:10.1038/nature09221

3. Chatelain E. Chagas disease research and development: Is there light at the end of the tunnel? Comput Struct Biotechnol J. 2017;15: 98–103. doi:10.1016/j.csbj.2016.12.002

4. Zuma AA, Dos Santos Barrias E, De Souza W. Basic Biology of Trypanosoma cruzi. Curr Pharm Des. 2021;27: 1671–1732. doi:10.2174/1381612826999201203213527

5. Cruz-Saavedra L, Vallejo GA, Guhl F, Ramírez JD. Transcriptomic changes across the life cycle of *Trypanosoma cruzi II*. PeerJ. 2020;8: e8947. doi:10.7717/peerj.8947

6. Teixeira SMR, DaRocha WD. Control of gene expression and genetic manipulation in the Trypanosomatidae. Genet Mol Res. 2003;2: 148–158.

7. Clayton C. Regulation of gene expression in trypanosomatids: living with polycistronic transcription. Open Biol. 2019;9: 190072. doi:10.1098/rsob.190072

8. Herreros-Cabello A, Callejas-Hernández F, Gironès N, Fresno M. Trypanosoma cruzi genome: Organization, multi-gene families, transcription, and biological implications. Genes. 2020;11: 1–26. doi:10.3390/genes11101196

9. Fleck K, Nitz M, Jeffers V. “Reading” a new chapter in protozoan parasite transcriptional regulation. Kafsack BFC, editor. PLOS Pathog. 2021;17: e1010056. doi:10.1371/journal.ppat.1010056

10. Martínez-Calvillo S, Vizuet-De-Rueda JC, Florencio-Martínez LE, Manning-Cela RG, Figueroa-Angulo EE. Gene expression in trypanosomatid parasites. J Biomed Biotechnol. 2010;2010. doi:10.1155/2010/525241

11. Smith SG, Zhou M-M. The Bromodomain as the Acetyl-Lysine Binding Domain in Gene Transcription. In: Zhou M-M, editor. Histone Recognition. Cham: Springer International Publishing; 2015. pp. 1–26. doi:10.1007/978-3-319-18102-8_1

12. Shi J, Vakoc CR. The Mechanisms behind the Therapeutic Activity of BET Bromodomain Inhibition. Mol Cell. 2014;54: 728–736. doi:10.1016/j.molcel.2014.05.016

13. Pezza A, Tavernelli LE, Alonso VL, Perdomo V, Gabarro R, Prinjha R, et al. Essential Bromodomain *Tc* BDF2 as a Drug Target against Chagas Disease. ACS Infect Dis. 2022;8: 1062–1074. doi:10.1021/acsinfecdis.2c00057

14. Alonso VL, Ritagliati C, Cribb P, Serra EC. Construction of three new gateway® expression plasmids for Trypanosoma cruzi. Mem Inst Oswaldo Cruz. 2014;109: 1081–1085. doi:10.1590/0074-0276140238

15. Ritagliati C, Villanova GV, Alonso VL, Zuma AA, Cribb P, Motta MCM, et al. Glycosomal bromodomain factor 1 from Trypanosoma cruzi enhances trypomastigote cell infection and intracellular amastigote growth. Biochem J. 2016;473: 73–85. doi:10.1042/BJ20150986

16. Rodriguez Araya E, Merli ML, Cribb P, De Souza VC, Serra E. Deciphering Divergent Trypanosomatid Nuclear Complexes by Analyzing Interactomic Datasets with AlphaFold2 and Genetic Approaches. ACS Infect Dis. 2023;9: 1267–1282. doi:10.1021/acsinfecdis.3c00148

17. Devoucoux M, Roques C, Lachance C, Lashgari A, Joly-Beauparlant C, Jacquet K, et al. MRG Proteins Are Shared by Multiple Protein Complexes With Distinct Functions. Mol Cell Proteomics. 2022;21: 100253. doi:10.1016/j.mcpro.2022.100253

18. Doyon Y, Selleck W, Lane WS, Tan S, Côté J. Structural and Functional Conservation of the NuA4 Histone Acetyltransferase Complex from Yeast to Humans. Mol Cell Biol. 2004;24: 1884–1896. doi:10.1128/MCB.24.5.1884-1896.2004

19. Saha S. Histone Modifications and Other Facets of Epigenetic Regulation in Trypanosomatids: Leaving Their Mark. Li Z, Garsin DA, editors. mBio. 2020;11: e01079-20. doi:10.1128/mBio.01079-20

20. Duraisingh MT, Horn D. Epigenetic Regulation of Virulence Gene Expression in Parasitic Protozoa. Cell Host Microbe. 2016;19: 629–640. doi:10.1016/j.chom.2016.04.020

21. Pezza A, Tavernelli LE, Alonso VL, Perdomo V, Gabarro R, Prinjha R, et al. Essential bromodomain TcBDF2 as a drug target against Chagas disease.

22. Belew AT, Junqueira C, Rodrigues-Luiz GF, Valente BM, Oliveira AER, Polidoro RB, et al. Comparative transcriptome profiling of virulent and non-virulent Trypanosoma cruzi underlines the role of surface proteins during infection. Taylor M, editor. PLOS Pathog. 2017;13: e1006767. doi:10.1371/journal.ppat.1006767

23. Kelly JM, Ward HM, Miles MA, Kendall G. A shuttle vector which facilitates the expression of transfected genes in Trypanosoma cruzi and Leishmania. Nucleic Acids Res. 1992 pp. 3963–3969. Available: https://academic.oup.com/nar/article/20/15/3963/2376634

24. Resende BC, Oliveira ACS, Guañabens ACP, Repolês BM, Santana V, Hiraiwa PM, et al. The Influence of Recombinational Processes to Induce Dormancy in Trypanosoma cruzi. Front Cell Infect Microbiol. 2020;10: 5. doi:10.3389/fcimb.2020.00005

25. Chiurillo MA, Lander N, Bertolini MS, Storey M, Vercesi AE, Docampo R. Different Roles of Mitochondrial Calcium Uniporter Complex Subunits in Growth and Infectivity of *Trypanosoma cruzi*. Sibley LD, editor. mBio. 2017;8: e00574-17. doi:10.1128/mBio.00574-17

26. Teixeira TL, Chiurillo MA, Lander N, Rodrigues CC, Onofre TS, Ferreira ÉR, et al. Ablation of the P21 Gene of Trypanosoma cruzi Provides Evidence of P21 as a Mediator in the Control of Epimastigote and Intracellular Amastigote Replication. Front Cell Infect Microbiol. 2022;12: 799668. doi:10.3389/fcimb.2022.799668

27. Costa-Silva HM, Resende BC, Umaki ACS, Prado W, Da Silva MS, Virgílio S, et al. DNA Topoisomerase 3α Is Involved in Homologous Recombination Repair and Replication Stress Response in Trypanosoma cruzi. Front Cell Dev Biol. 2021;9: 633195w. doi:10.3389/fcell.2021.633195

28. Silva-Gomes NL, Rampazzo RDCP, Moreira CMDN, Porcino GN, Santos CMBD, Krieger MA, et al. Knocking Down TcNTPDase-1 Gene Reduces in vitro Infectivity of Trypanosoma cruzi. Front Microbiol. 2020;11: 434. doi:10.3389/fmicb.2020.00434

29. Burle-Caldas GDA, Dos Santos NSA, De Castro JT, Mugge FLB, Grazielle-Silva V, Oliveira AER, et al. Disruption of Active Trans-Sialidase Genes Impairs Egress from Mammalian Host Cells and Generates Highly Attenuated Trypanosoma cruzi Parasites. Burleigh B, editor. mBio. 2022;13: e03478-21. doi:10.1128/mbio.03478-21

30. Staneva DP, Carloni R, Auchynnikava T, Tong P, Arulanandam JA, Rappsilber J, et al. A systematic analysis of Trypanosoma brucei chromatin factors identifies novel protein interaction networks associated with sites of transcription initiation and termination. bioRxiv. 2021; 2021.02.09.430399. Available: http://biorxiv.org/content/early/2021/02/10/2021.02.09.430399.1.abstract

31. Allard S. NuA4, an essential transcription adaptor/histone H4 acetyltransferase complex containing Esa1p and the ATM-related cofactor Tra1p. EMBO J. 1999;18: 5108–5119. doi:10.1093/emboj/18.18.5108

32. Squatrito M, Gorrini C, Amati B. Tip60 in DNA damage response and growth control: many tricks in one HAT. Trends Cell Biol. 2006;16: 433–442. doi:10.1016/j.tcb.2006.07.007

33. Hodges AJ, Plummer DA, Wyrick JJ. NuA4 acetyltransferase is required for efficient nucleotide excision repair in yeast. DNA Repair. 2019;73: 91–98.

doi:10.1016/j.dnarep.2018.11.006

34. Sánchez-Valdéz FJ, Padilla A, Wang W, Orr D, Tarleton RL. Spontaneous dormancy protects Trypanosoma cruzi during extended drug exposure. eLife. 2018;7: e34039. doi:10.7554/eLife.34039

35. Barrett MP, Kyle DE, Sibley LD, Radke JB, Tarleton RL. Protozoan persister-like cells and drug treatment failure. Nat Rev Microbiol. 2019;17: 607–620. doi:10.1038/s41579-019-0238-x

36. Bustamante JM, Sanchez-Valdez F, Padilla AM, White B, Wang W, Tarleton RL. A modified drug regimen clears active and dormant trypanosomes in mouse models of Chagas disease. Sci Transl Med. 2020;12: eabb7656. doi:10.1126/scitranslmed.abb7656

37. Bunkofske ME, Sanchez-Valdez FJ, Tarleton RL. The importance of persistence and dormancy in Trypanosoma cruzi infection and Chagas disease. Curr Opin Microbiol. 2025;86: 102615. doi:10.1016/j.mib.2025.102615

38. Rossetto D, Cramet M, Wang AY, Steunou A, Lacoste N, Schulze JM, et al. Eaf5/7/3 form a functionally independent NuA4 submodule linked to RNA polymerase II -coupled nucleosome recycling. EMBO J. 2014;33: 1397–1415. doi:10.15252/embj.201386433

39. Yamaguchi K, Nakagawa S, Furukawa Y. Understanding the role of BRD8 in human carcinogenesis. Cancer Sci. 2024;115: 2862–2870. doi:10.1111/cas.16263

40. Browne JA, NandyMazumdar M, Paranjapye A, Leir S-H, Harris A. The Bromodomain Containing 8 (BRD8) transcriptional network in human lung epithelial cells. Mol Cell Endocrinol. 2021;524: 111169. doi:10.1016/j.mce.2021.111169

41. Filippakopoulos P, Picaud S, Mangos M, Keates T, Lambert J-P, Barsyte-Lovejoy D, et al. Histone Recognition and Large-Scale Structural Analysis of the Human Bromodomain Family. Cell. 2012;149: 214–231. doi:10.1016/j.cell.2012.02.013

42. Lander N, Li ZH, Niyogi S, Docampo R. CRISPR/Cas9-induced disruption of paraflagellar rod protein 1 and 2 genes in Trypanosoma cruzi reveals their role in flagellar attachment. mBio. 2015;6: 1–12. doi:10.1128/mBio.01012-15

43. Lander N, Chiurillo MA, Docampo R. Genome editing by CRISPR/Cas9 in trypanosoma cruzi. Methods Mol Biol. 2019;1955: 61–76. doi:10.1007/978-1-4939-9148-8_5

44. Alonso VL. Ultrastructure Expansion Microscopy (U-ExM) in Trypanosoma cruzi: localization of tubulin isoforms and isotypes. Parasitol Res. 2022;121: 3019–3024. doi:10.1007/s00436-022-07619-z

45. De Hernández MA, Martinez Peralta G, Vena R, Alonso VL. Ultrastructural Expansion Microscopy in Three In Vitro Life Cycle Stages of Trypanosoma cruzi. J Vis Exp. 2023; 65381. doi:10.3791/65381

46. Perdomo V, Boselli V, Manarin R, Serra E. Optimizing In Vitro Metacyclogenesis: Strain-Specific Variability in Trypanosoma cruzi Responses to Nutritional and pH Stress. 2025.

47. Rodrigues JPF, Souza Onofre T, Barbosa BC, Ferreira ÉR, Bonfim-Melo A, Yoshida N. Host cell protein LAMP-2 is the receptor for *Trypanosoma cruzi* surface molecule gp82 that mediates invasion. Cell Microbiol. 2019;21: e13003. doi:10.1111/cmi.13003

48. Andrade LO, Andrews NW. The Trypanosoma cruzi–host-cell interplay: location, invasion, retention. Nat Rev Microbiol. 2005;3: 819–823. doi:10.1038/nrmicro1249

49. Romano PS, Cueto JA, Casassa AF, Vanrell MC, Gottlieb RA, Colombo MI. Molecular and cellular mechanisms involved in the *Trypanosoma cruzi* /host cell interplay. IUBMB Life. 2012;64: 387–396. doi:10.1002/iub.1019

50. Brener Z. Therapeutic activity and criterion of cure on mice experimentally infected with Trypanosoma cruzi. Rev Inst Med Trop Sao Paulo. 1962;4: 389–396.

51. Cummings KL, Tarleton RL. Rapid quantitation of Trypanosoma cruzi in host tissue by real-time PCR. Mol Biochem Parasitol. 2003;129: 53–59. doi:10.1016/S0166-6851(03)00093-8

52. Duffy T, Bisio M, Altcheh J, Burgos JM, Diez M, Levin MJ, et al. Accurate Real-Time PCR Strategy for Monitoring Bloodstream Parasitic Loads in Chagas Disease Patients. Rodriguez A, editor. PLoS Negl Trop Dis. 2009;3: e419. doi:10.1371/journal.pntd.0000419